ORIGINAL ARTICLE

CLINICAL ORAL IMPLANTS RESEARCH WILEY

Osteoinductive calcium phosphate with submicron topography as bone graft substitute for maxillary sinus floor augmentation: A translational study

Lukas A. van Dijk[1,2,3] | Nard G. Janssen[1] | Silke J. Nurmohamed[1] |
Marvick S. M. Muradin[1] | Alessia Longoni[1,2] | Robbert C. Bakker[1] |
Florence G. de Groot[3] | Joost D. de Bruijn[3,4] | Debby Gawlitta[1,2] |
Antoine J. W. P. Rosenberg[1]

[1]Department of Oral and Maxillofacial Surgery, University Medical Center Utrecht, Utrecht, the Netherlands

[2]Regenerative Medicine Center Utrecht, Utrecht, the Netherlands

[3]Kuros Biosciences BV, Bilthoven, the Netherlands

[4]School of Materials Science and Engineering, Queen Mary University of London, London, UK

Correspondence
Lukas A. van Dijk, Department of Oral and Maxillofacial Surgery, University Medical Center Utrecht, Utrecht, the Netherlands.
Email: luuk.van.dijk@kurosbio.com

Funding information
H2020 European Institute of Innovation and Technology, Grant/Award Number: 674282, 874790 and 953169

Abstract

Objectives: The aim of this study was the preclinical and clinical evaluation of osteoinductive calcium phosphate with submicron surface topography as a bone graft substitute for maxillary sinus floor augmentation (MSFA).

Material and Methods: A preclinical sheep model of MSFA was used to compare a calcium phosphate with submicron needle-shaped topography (BCP_N, MagnetOs Granules, Kuros Biosciences BV) to a calcium phosphate with submicron grain-shaped topography (BCP_G) and autologous bone graft (ABG) as controls. Secondly, a 10-patient, prospective, randomized, controlled trial was performed to compare BCP_N to ABG in MSFA with two-stage implant placement.

Results: The pre-clinical study demonstrated that both BCP_N and BCP_G were highly biocompatible, supported bony ingrowth with direct bone apposition against the material, and exhibited bone formation as early as 3 weeks post-implantation. However, BCP_N demonstrated significantly more bone formation than BCP_G at the study endpoint of 12 weeks. Only BCP_N reached an equivalent amount of bone formation in the available space and a greater proportion of calcified material (bone + graft material) in the maxillary sinus compared to the "gold standard" ABG after 12 weeks. These results were validated in a small prospective clinical study, in which BCP_N was found comparable to ABG in implant stability, bone height, new bone formation in trephine core biopsies, and overall clinical outcome.

Conclusion: This translational work demonstrates that osteoinductive calcium phosphates are promising bone graft substitutes for MSFA, whereas their bone-forming potential depends on the design of their surface features.

Netherlands Trial Register, NL6436.

KEYWORDS
bone graft substitutes, clinical study, osteoinductive calcium phosphate, preprosthetic dental surgery, sinus floor augmentation, submicron surface topography, translational research bone regeneration

1 | INTRODUCTION

Endosseous dental implants are frequently employed to achieve esthetic and functional restoration of missing teeth and molars. Rehabilitation of the posterior maxilla using dental implants is often challenging due to the prevalence of inadequate quality and quantity of alveolar bone as a result of post-extraction bone resorption and sinus pneumatization (Sharan & Madjar, 2008; Tolstunov et al., 2012). Maxillary sinus floor augmentation (MSFA) is performed for almost 40% of posterior maxillary implants to restore the bone mass required for implant insertion and integration (Danesh-Sani et al., 2016; Tomruk et al., 2016). In general, the procedure has been associated with favorable short- and long-term outcomes in terms of implant survival (Raghoebar et al., 2019). Autologous bone grafts (ABGs), which may be harvested from the iliac crest, calvarium, or from local sites, that is, chin or intra-oral bone, are considered the "gold standard" graft material for MSFA due to their osteogenic, osteoinductive, and osteoconductive properties (Roberts & Rosenbaum, 2012). However, ABG harvesting from the iliac crest or calvarium donor sites is associated with donor site morbidity, extended operating times and costs (Gjerde et al., 2020; Truedsson et al., 2013). Also, some donor sites provide for limited availability of bone (Klijn et al., 2010b). Furthermore, significant early graft resorption has been reported with the use of ABG for maxillary bone augmentation (Emeka & Neukam, 2014; Johansson et al., 2001).

A variety of bone graft substitutes has been developed to overcome these limitations for MSFA, including allografts, xenografts, and alloplastic or synthetic bone substitutes, which all consist of calcified matrices that comprise or mimic the mineral phase of bone (Haugen et al., 2019; Roberts & Rosenbaum, 2012). An important benefit of such bone substitutes is that they can be used off-the-shelf, surpassing the invasive harvesting procedures of ABG. However, while the use of bone graft substitutes in MSFA is generally recommended, variable outcomes have been reported when compared to ABG in clinical settings (Haugen et al., 2019; Papageorgiou et al., 2016). As developments in the field of bone graft substitutes continue to advance, screening of novel bone graft substitute materials as a treatment option for MSFA remains an important research aim.

A disadvantage of most bone substitutes is that they are predominantly osteoconductive and thus rely on bone ingrowth from the bone surrounding the defect (Roberts & Rosenbaum, 2012). However, recent efforts to improve the efficacy of calcium phosphate bone graft substitutes have resulted in materials with substantial osteoinductive capacity, demonstrated by their ability to induce bone formation in non-osseous soft tissues, that is, intramuscularly, as published previously by our group, and others. (Duan et al., 2016; Duan et al., 2019; Duan, Barbieri, De Groot, et al., 2018; Duan, Barbieri, Luo, et al., 2018; Le Nihouannen et al., 2005; Yuan et al., 2010). Harboring both osteoconductive and osteoinductive properties, these calcium phosphates meet two out of the three essential properties that ABGs possess (Roberts & Rosenbaum, 2012). These materials have been reliably demonstrated to enhance bone healing when compared to materials with mere osteoconductive capacity, and have shown equivalence to ABG in orthotopic defects (Duan et al., 2016; Duan, Barbieri, De Groot, et al., 2018; Habibovic et al., 2006; van Dijk et al., 2018; Van Dijk et al., 2020; Yuan et al., 2010). Moreover, excellent results have been achieved with clinical use of osteoinductive calcium phosphates, such as their use for alveolar cleft reconstruction in patients with cleft lip and palate and related craniofacial anomalies (De Ruiter et al., 2015; Janssen et al., 2019) and in extraction sockets in anterior maxilla regions with immediate implant placement in the esthetic zone (Barroso-Panella et al., 2018). Osteoinductive materials also have potential for use in MSFA, as they may promote faster and more extensive bone formation than conventional materials, which could ultimately benefit implant osseointegration.

The biocompatibility and performance of bone substitute biomaterials, including calcium phosphates, are dependent on their physicochemical properties, which include phase composition, micro- and macroporosity, and surface topography. Osteoinductive capacity has been shown to vary strongly between different calcium phosphate-based materials. It has been repeatedly demonstrated that a critical factor for osteoinductive capacity is the presence of a submicron surface topography, that is, a topography of elongated surface crystals smaller than 1 μm in diameter (Duan et al., 2016; Duan et al., 2019; Duan, Barbieri, De Groot, et al., 2018; Duan, Barbieri, Luo, et al., 2018; Yuan et al., 2010). Moreover, we have recently demonstrated that besides dimension, the needle-like shape of submicron surface crystals can influence osteoinductive capacity (Duan et al., 2019).

The aim of the present work was to evaluate osteoinductive calcium phosphate with submicron surface topography as a bone graft substitute for MSFA, in both a pre-clinical study in a sheep model and a prospective, randomized, controlled clinical trial. In the pre-clinical study, two different biphasic calcium phosphate materials with submicron topography were compared to the "gold standard" iliac crest-derived ABG. The synthetic bone substitutes exhibited either needle-shaped (BCP$_N$) or grain-shaped (BCP$_G$) submicron surface crystal morphology. MSFA treatment outcomes were assessed using micro-computed tomography (micro-CT) and histology after 3, 6, and 12 weeks of healing. The clinical study was a prospective, open-label, randomized, controlled trial in which the BCP$_N$ bone substitute was compared to ABG in a cohort of 10 patients receiving lateral window MSFA with two-stage implant placement. Outcome measures during 17 months of follow-up included implant stability, bone height by radiography, the histology and histomorphometry of trephine bone core biopsies, and clinical outcomes.

2 | MATERIALS AND METHODS

2.1 | In vivo evaluation in a sheep MSFA model

2.1.1 | Bone graft substitutes

Two commercially available, calcium phosphate bone substitute materials were evaluated in this study. Both materials were used as

porous granules, featuring a submicron topography (Figure 1), that is, a surface crystal diameter <1 μm, and were of biphasic composition, that is, consisting of ß-tricalcium phosphate (ßTCP or $Ca_3(PO_4)_2$) and hydroxyapatite (HA - $Ca_{10}(PO_4)_6 \cdot (OH)_2$).

In brief, the first formulation, BCP_N (MagnetOs™, Kuros Biosciences BV, the Netherlands), had a surface topography of submicron needle-shaped crystals and a phase composition of 70% βTCP and 30% HA. The granule size range was 0.25–1 mm. The second formulation, BCP_G, (MBCP™, Biomatlante, France), had a topography of submicron grain-shaped crystals, a composition of 60% βTCP / 40% HA and a granule size of 0.5–1 mm. Both materials were sterile and used according to the manufacturer's instructions for use. Figure 1 shows the surface features of BCP_N and BCP_G as observed by scanning electron microscope. The material properties of BCP_N and BCP_G are detailed in Table S1.

2.1.2 | Animals

Following approval of the study protocol by the Central Authority for Scientific Procedures on Animals (Dutch national CCD, under AVD115002015344), 24 sheep (*Ovis Aries*) were admitted to the study. All animals were female, had reached maturity (ages 3–6 years), and weighed between 60 and 100 kg. The animals were randomized into 3 groups for 3-, 6-, and 12-week follow-up periods, with 6, 9, and 9 animals per group, respectively. No animals were excluded. Animals were housed at the "Gemeenschappelijk Dierenlaboratorium" in Utrecht. Animal housing and care was compliant with the national guidelines and regulations. A weight loss of >20% (checked weekly), severe wound abscess (checked daily), or strongly reduced mobility (checked daily) were used as humane endpoints. An experimental timeline of the study is shown in Figure 2(a). This study was compliant with the ARRIVE guidelines.

2.1.3 | Surgical procedure

Bilateral MSFA in this sheep model was performed following the lateral window approach, as previously described (Hoekstra et al., 2013). Prior to surgery, animals were pre-medicated with the analgesics buprenorphine (*t.d.* 5 μg/h) and meloxicam (*i.v.* 0.5 mg/ kg) and the antibiotic amoxicillin/clavulanic acid (*i.v.* 10 mg/kg). Anesthesia was initiated with detomidine (*i.m.* 0.05 mg/kg) and

propofol (*i.v.* 5–7 mg/kg) and was maintained with propofol (*i.v.* 10 mg/kg/h) and sufentanil (*i.v.* 0.003 mg/kg/h). Animals were connected to an inhalation ventilator and positioned in sternal recumbency. Operation sites were washed, shaved, disinfected, and sterile drapes were applied. Corticocancellous ABG was harvested from the iliac crest and was reduced to 2–5 mm particles. The maxillary sinuses were approached via the facial lateral wall, which was exposed by sharp and blunt dissection. Using a high-speed dental burr, a bony window of $\pm 1 \times 1\ cm^2$ was created under continuous irrigation, taking care not to perforate the underlying Schneiderian membrane. After removal of the bony window, the Schneiderian membrane was carefully elevated with blunt dissectors, to expose the bony surface of the maxillary sinus floor and walls. Next, 2 cc of either ABG, BCP_N, or BCP_G was implanted on the exposed maxillary sinus floor. Both BCP_N and BCP_G were mixed with 1–2 cc of local blood prior to implantation to improve handling. Each animal received a bilateral implantation, and the three graft/substitute materials were assigned in a randomized manner for each timepoint (3 weeks [$n = 4$], 6 weeks [$n = 6$], and 12 weeks [$n = 6$]). The soft tissues at the surgical site were closed in layers using resorbable sutures (Vicryl 3–0, Ethicon, Brussels, Belgium). After surgery, animals received meloxicam (*s.c.* 0.5 mg/kg, 1×/day for 3 days) for pain management and penicillin-neomycin (0.05 mg/kg, 1×/day for 3 days) as an antibiotic, in addition to standard care and monitoring.

2.1.4 | Calcium-binding fluorochrome labeling

Polychrome sequential labeling with calcium-binding fluorochromes was performed on the 12-week group in order to visualize active sites of mineralization during bone formation. Treatment with three different fluorescent calcium-binding labels was performed, one at each time point. The sequentially injected fluorochrome labels used were calcein at 3 weeks (CN, 10 mg/kg, *i.v.*—green), xylenol orange at 6 weeks (XO, 90 mg/kg, *i.v.*—red) and oxytetracycline at 9 weeks (OTC, 20 mg/kg, *i.m.*—yellow), respectively.

2.1.5 | Sample harvesting and processing

After reaching the experimental endpoint, animals were euthanized with pentobarbital. The maxillary sinuses were excised, trimmed, and fixed in 4% formaldehyde solution for 1 week at 4°C. The
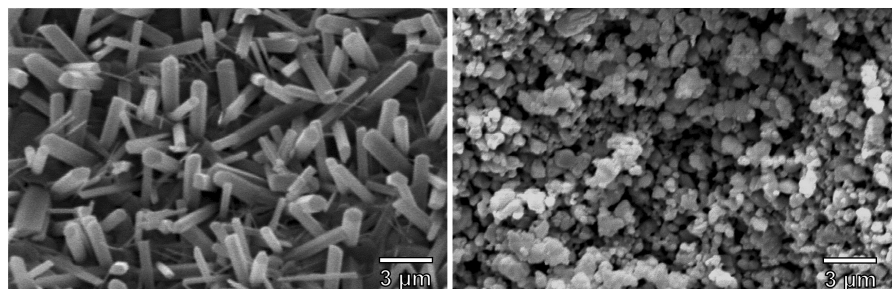

FIGURE 1 SEM micrographs of the submicron topography on BCP_N and BCP_G. The different morphologies of submicron surface crystals are evident, with needle-shaped crystals on BCP_N and grain-shaped crystals on BCP_G.
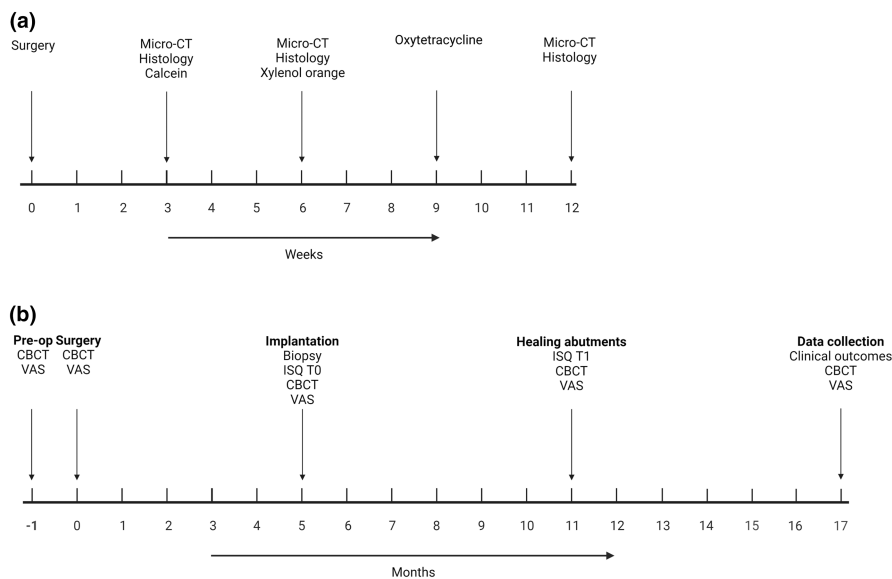
(a)

(b)

FIGURE 2 Study timelines. (a) Experimental timeline for the sheep MSFA study. (b) Study timeline of the clinical MSFA trial.

samples were then dehydrated through a series of increasing ethanol concentrations (70%–100%) and subsequently embedded in polymethyl-methacrylate (PMMA).

2.1.6 | Micro-computed tomography

PMMA-embedded samples were scanned in micro-CT scanner (QuantumFX, Perkin Elmer) with a voxel size of $59 \times 59 \times 59\,\mu m^3$, voltage at 90 kV, and a tube current of 180 μA. On TIFF stacks derived from the scans, vertical bone height was measured in the bucco-palatal plane at the center of each graft, in a straight line from the lowest level of the sinus floor to the highest level of the graft, using dedicated software (3D Slicer 4.10).

2.1.7 | Histology

A Leica SP1600 saw microtome was used to cut ~15-micron thick sections from the center of each graft in the bucco–palatal direction. On these sections, a histological staining of methylene blue (Sigma; 1% in 0.1 M borax buffer, pH 8.5) and basic fuchsin (Sigma; 0.3% in demi water) was performed to visualize bone tissue (bone matrix: pink, fibrous tissues: blue). Sections were examined under a Leica microscope (Eclipse 50i; Nikon) and scanned with a slide scanner (DiMage scan 5400 Elite II; Konica Minolta).

A fluorescence microscope (BX51, Olympus) was used to visualize fluorochrome label deposition in otherwise unstained sections. Fluorescent signals in each section were captured using appropriate excitation and emission wavelength filters for CN (ex:436–495, em:517–540), XO (ex:377–570, em:610–615), and OTC (ex:365–490, em:520–570). The polychrome fluorescent signals were then digitally merged with a transmission light microscopy image (15% opacity) using software (Adobe Photoshop CS5) to visualize the deposition of each label in the sections.

2.1.8 | Histomorphometry

Histomorphometry of methylene blue/basic fuchsin-stained PMMA sections was performed on digitalized scans by pseudo-coloring of pixels representing bone (B; mineralized + osteoid) and bone graft material (M, only for bone graft substitutes) in the entire area of new bone formation as region of interest (ROI). The examiners were blinded for the treatments. The number of pixels for B, M, and ROI were used to calculate the area percentage of bone in the available space using the following formula: $B/(ROI - M) \times 100$. In addition, the area percentage of remaining implant material was calculated by the following formula: $M/ROI \times 100$. Lastly, the combined proportion of bone + material was calculated by: $(B+M)/ROI \times 100$.

2.2 | Evaluation in a clinical MSFA study

2.2.1 | Study design

This was a single-center, prospective, open-label, randomized controlled trial conducted at a university hospital in the Netherlands, at the department of Oral and Maxillofacial Surgery. Ethical approval was provided by the Medical Research Ethics Committee Utrecht (NL61242.041.17), in accordance with the principles of the Declaration of Helsinki (version October 2008) and the Medical Research Involving Human Subjects Act. Each participant provided written informed consent after receiving adequate verbal and written explanations prior to inclusion in the study. Based on computerized block randomization (1:1), patients were allocated to the parallel treatment arms of the test group, BCP_N, or the control group, ABG. Study investigators were blinded for the treatment allocation, apart from the treating clinicians and study coordinator. A timeline of the study is presented in Figure 2b. The study was designed as a non-inferiority trial, but it did not reach

full inclusion and was underpowered, so the non-inferiority hypothesis was not tested.

2.2.2 | Study inclusion criteria

The most important inclusion criteria were age between 18 and 75 years and participants qualifying for MSFA with two-stage implant placement. Indications for surgery were the presence of a unilateral or bilateral (partial) atrophic posterior maxilla in the premolar/molar areas, with a residual vertical bone height between 2 and 6 millimeters. The full inclusion and exclusion criteria of the study are presented in the appendix, Table S2.

2.2.3 | Intervention

MSFA was performed using the lateral-window technique with a trapdoor approach to access the sinus and elevate the Schneiderian membrane. Depending on the treatment arm, the thus created sub-Schneiderian void was implanted with BCP_N granules of 0.25–1 mm or morselized autograft harvested locally (i.e., mandibular ramus) or from the iliac crest. The amount of graft or material used depended on the individual's sinus volume, the desired vertical height, and the number of planned implants per side. The surgery was ended by replacement of the mucoperiosteal flap and primary wound closure.

Primary implant placement was performed after 5 months of healing. During osteotomy of the implant bed, a trephine core bone biopsy was harvested using a trephine burr (2 mm internal/3 mm external diameter, Meisinger, Neuss, Germany). The trephine core biopsies were preserved in 10% formalin and stored until histological processing. After implant insertion (OsseoSpeed® EV, Astra Tech Implant System, Dentsply Sirona Implants, Mölndal, Sweden), cover screws were installed on the fixtures and primary wound closure was attained. After another 6 months of healing, at 11 months follow-up, patients were invited to the outpatient clinic for the installation of healing abutments. The prosthetic restorations were installed after the soft tissues had healed. Following another 6 months, at 17 months follow-up, the patients were invited to the outpatient clinic for a final visit, during which a clinical assessment of peri-implant health was performed. At all study visits throughout the follow-up period, a cone beam computed tomography (CBCT) scan was made.

2.2.4 | Outcome measures

Implant stability

Implant stability quotient (ISQ) of dental implants in the posterior maxilla was measured by resonance frequency analysis (RFA) using the Penguin^{RFA} system (Integration Diagnostics AB, Gothenburg, Sweden). Primary stability was recorded immediately after implantation (T0, 5 months), and secondary stability was measured prior to the installation of the healing abutments (T1, 11 months). The intra-implant difference in primary and secondary stability was calculated using the formula $\Delta ISQ = ISQ_{T1} - ISQ_{T0}$.

Bone height

The bone height of the maxillary sinus floor was measured by CBCT pre-operatively (baseline), post-operatively, and at 5, 11, and 17 months of follow-up.

New bone formation

Formalin-fixed trephine core biopsies were decalcified in ethylenediaminetetraacetic acid (EDTA), dehydrated using an ethanol series and embedded in paraffin for histology. Specimens were sectioned using a microtome and subsequently stained with hematoxylin and eosin. Sections were examined under a Leica microscope (Eclipse 50i; Nikon) and were scanned with a slide scanner (DiMage scan 5400 Elite II; Konica Minolta).

Histomorphometry of biopsy sections was performed on the digitalized scans by pseudo-coloring of pixels representing bone (B) and remaining material (M, only for BCP_N,) in the ROI using Photoshop (Photoshop CS5). The area percentage of bone and remaining implant material was calculated as described for the sheep study.

Clinical outcomes

Clinical outcomes included implant survival rate, adverse events, and pain by a visual analog scale (0–100) recorded on all visits throughout the follow-up period. Moreover, peri-implant health was assessed after 17 months of follow-up using the gingival index (Löe & Silness, 1963), supra-gingival plaque index (Silness & Löe, 1964), and dichotomous bleeding index. Lastly, the probing depth of the implants in the posterior maxilla was also measured after 17 months of follow-up (buccal, palatal, mesial, and distal).

Statistical analysis

For the animal study, sample size was determined using Russ Lenth's software tool, based on a statistical power of 80%, a p-value of .05, a standard deviation of 17.5%, and a contrast of means of 0.3, considering one-way Analysis of Variance for new bone formation (histomorphometry) (Lenth Russ, 2006). The clinical study was designed as a non-inferiority trial for 26 patients, but it did not reach full inclusion, and the non-inferiority hypothesis was not tested, because the study was underpowered. All data are presented as mean ± standard deviation. Quantitative data were analyzed using statistical analysis software, Graphpad Prism (version 7, Graphpad). The normal distribution of the data was tested by the Shapiro–Wilk normality test. In the preclinical study, all data were analyzed using Two-way Analysis of Variance, followed by the Holm-Sidak test for post hoc analysis. In the clinical study, implant stability was also analyzed using Two-way Analysis of Variance, followed by the Holm-Sidak test for post hoc analysis. The clinical bone height data were analyzed using a Repeated Measures Analysis of Variance, with a Holm-Sidak test for post hoc analysis. All other data in the clinical study were analyzed

using the Mann–Whitney U test (for non-normal data) or Fisher's exact test (for categorical data). A significance level of $p < .05$ was used. The following notation was used to indicate statistical significance: $*p < .05$, $**p < .01$, $***p < .001$.

3 | RESULTS

3.1 | Sheep MSFA model

All MSFA surgeries and graft implantations were completed uneventful. The animals recovered without complications and all reached the final endpoint in healthy condition. In all groups, no adverse reactions to the graft materials were observed.

3.1.1 | Micro-CT

On micro-CT scans (Figure 3a,b), the implanted bone substitutes were localized beneath the Schneiderian membrane in direct contact with the bony floor of the maxillary sinus and walls. In all groups, the implants were contained at their implantation sites, and there was no evidence of graft migration. Over time, the ABG particles remodeled and fused to one another and onto the host bone surfaces, resulting in a solid trabeculated bone mass at 12 weeks. For the synthetic bone substitutes, progressive mineralized growth into the implants could be observed over time. For both bone substitutes, the mineralized matrix gradually invaded the intergranular space, resulting in compact, consolidated grafts at the 12 week timepoint. Some specimens of BCP_N and BCP_G showed regions without mineralized ingrowth after 12 weeks, often located near the lateral window or in the superior aspect of the graft, that is, regions most distant from the host bone surfaces. Overall, the augmentations with the synthetic grafts appeared to have more volume compared to ABG implants.

Vertical augmentation height (Figure 3c) of the different graft types was measured on micro-CT scans to determine MSFA success and graft stability during the follow-up period. The augmentation height range was 5.31–11.52 mm for ABG, 8.67–16.98 mm for BCP_N and 8.97–14.46 mm for BCP_G. At each timepoint, the
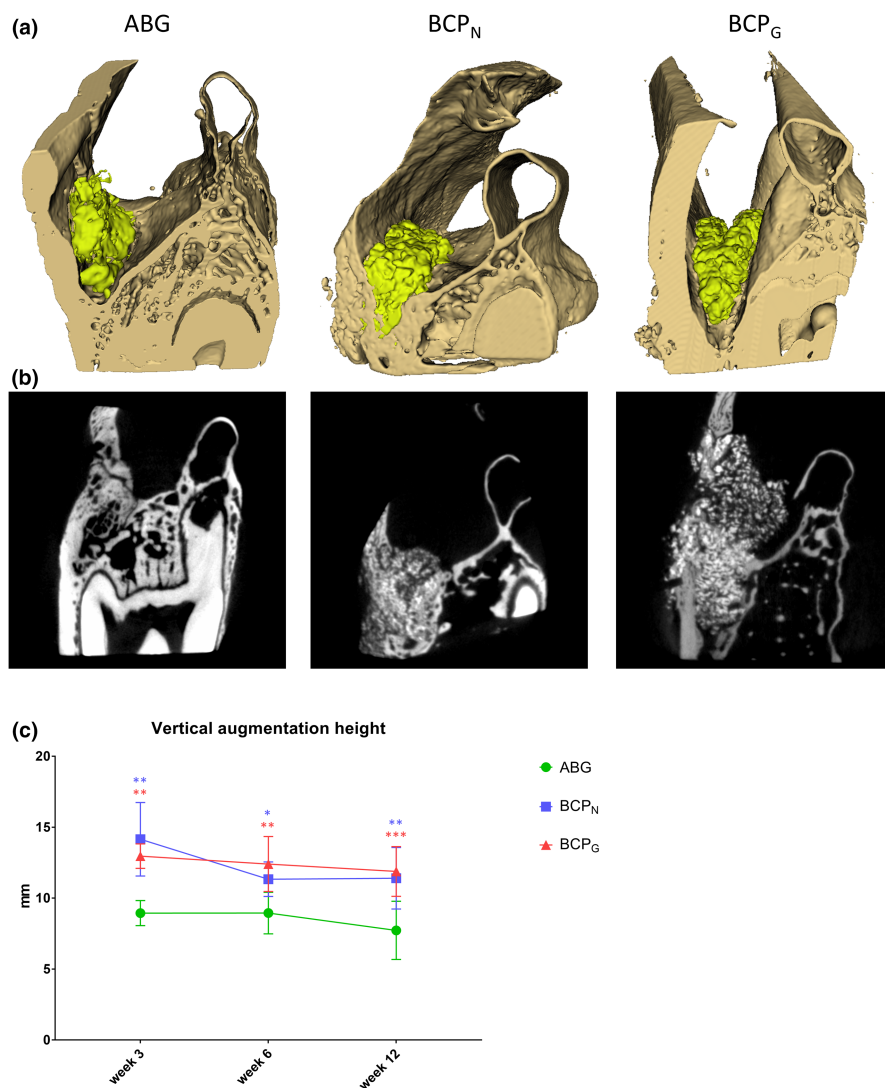
FIGURE 3 Evaluation of MSFA by micro-CT. (a) Representative 3D reconstructions of bone grafts (yellow) implanted beneath the Schneiderian membrane on the bony floor of the maxillary sinus after 12 weeks of healing. The bone grafts can be observed in contact with the host bony sinus floor and walls (off-white). (b) Representative micro-CT slices from the center of the implanted grafts at 12 weeks. Radiodense calcium phosphate granules and mineralized bone matrix can be observed. The more homogeneous regions in BCP_N and BCP_G specimens represent integration of calcium phosphate in the new mineralized bone matrix. (c) Vertical augmentation height, as measured by micro-CT in the center of the grafts at week 3, 6 and 12. Blue asterisks indicate significance for BCP_N vs ABG, red asterisks for BCP_G vs ABG.

augmentation height of BCP$_N$ and BCP$_G$ was significantly higher than that of ABG, while the two synthetic bone substitutes did not result in significantly different heights from each other. After 12 weeks of follow-up, the difference in mean augmentation height between the synthetic bone substitutes (BCP$_N$: 11.88 ± 2.17 mm; BCP$_G$ 11.40 ± 1.75 mm) and ABG (7.73 ± 2.05 mm) was ± 4.0 mm, corresponding to roughly 1.5-fold greater augmentation height for the synthetic implants versus ABG. All graft types demonstrated a decreasing trend in augmentation height between 3 and 12 weeks, being the largest for BCP$_N$ (2.75 mm), followed by ABG (1.22 mm) and BCP$_G$ (1.08 mm).

3.1.2 | Histology

Histological analyses were performed to complement the micro-CT data and further investigate new bone formation in the implants. On low magnification histological overviews (Figure 4a) of ABG specimens, individual ABG segments could still be clearly distinguished at the 3-week timepoint, while embedded in a matrix of fibrous tissue. The initiation of new bone formation on the surface of the ABG particles as well as on the sinus floor and walls could be observed. After 6 weeks, the individual bone pieces were more interconnected as a result of new bone formation. By 12 weeks, the ABG implants had consolidated into a single, interconnected bone mass and were fused to the bony floor of the sinus. The proportion of newly formed and remodeled bone had increased, although original ABG fragments could still be recognized. Regions of fibrous tissue could still be discerned in the graft area after 12 weeks.

For the synthetic bone graft substitutes, calcium phosphate granules could be recognized on the histological sections (Figure 4a). On low magnification histological overviews of 3-week specimens, the graft materials were entirely embedded in soft tissue, and early osteoconductive bone ingrowth originating from the host bone could be observed with both materials. Interestingly, 2/3 samples of BCP$_N$ and 1/4 of BCP$_G$ exhibited regions with new bone in areas at the center of the graft or near the Schneiderian membrane (Figure 4b). Further progression of bone formation was observed at 6 weeks, while at 12 weeks, mineralized bone was bridging between granules throughout the grafts, resulting in a trabeculated, interconnected mass of bone and calcium phosphate particles. As with ABG, specimens of either synthetic material presented local regions with fibrous tissue after 12 weeks.

High magnification microscopy of BCP$_N$ and BCP$_G$ specimens (Figure 5) revealed new bone formation around and directly against BCP particles at 3 weeks. The presence of ample osteoblasts actively depositing osteoid as well as a woven bone morphology were indicative of ongoing primary osteogenesis. No adverse tissue reactions to the synthetic implants were observed. A lamellar bone phenotype was observed at 6 weeks, demonstrating that the woven bone matrix was remodeled into mature, secondary bone tissue. BCP granules were progressively engulfed by the ongoing bone formation process that incorporated them in the mineralized bone matrix. After 12 weeks, sites of new bone deposition were less frequently observed. By this time, the regions between BCP granules were predominantly occupied by dense lamellar bone matrix that bridged the adjacent granules. Overall, the bone tissue that had formed around both synthetic materials had all the characteristics of normal, healthy bone tissue, including bone marrow spaces, concentric lamellae, osteocytes, and capillaries. Large, phagocytosing multinucleated cells were frequently observed on the exposed surfaces of either BCP material at all timepoints. Degraded BCP material was commonly observed in the cytoplasm of these cells, indicating their ability to actively resorb the BCP material (Figure 5g,h).

3.1.3 | Histomorphometry

Histomorphometry performed on histological sections allowed the quantitative analysis of bone formation in the implants over time (Figure 6). Morphometry of the bone matrix (Figure 6a) revealed a higher area percentage of bone in the available space for ABG compared to the synthetic grafts at 6 weeks. It must be noted that the percentage of bone in the ABG specimens includes the implanted autograft particles as well as newly formed bone, whereas for the synthetic materials, it only includes newly formed bone. At the study endpoint at 12 weeks, bone formation in BCP$_N$ (38.3 ± 9.8%) was comparable to the ABG control (44.0 ± 8.5%). However, with BCP$_G$, the percentage of bone formation at 12 weeks (26.8 ± 11.4%) was 11.4% lower than BCP$_N$ and 17.2% lower than ABG. This corresponded to approximately one-third less bone formation in the available space for BCP$_G$ than with ABG and BCP$_N$. Area percentages occupied by BCP$_N$ and BCP$_G$ bone graft substitute materials were equivalent at all timepoints (Figure 6b). The area percentages of both graft materials did not follow a negative trend with time, which could have indicated material resorption. When combining bone and calcium phosphate graft material (Figure 6c), the area percentage for the bone substitutes was greater than for ABG at 3 and 6 weeks. After 12 weeks, the area percentage of combined bone and graft material was only higher in BCP$_N$ (60.3% ± 5.5%) versus ABG (44.0% ± 8.5%).

3.1.4 | Fluorochrome label analysis

Intra-animal bone formation dynamics were analyzed by observation of the deposition of sequentially injected calcium-binding fluorochrome labels using fluorescence microscopy (Figure 7). The presence of the fluorochrome label CN (3 weeks, green) in the majority of BCP$_N$ and BCP$_G$ specimens indicated that the onset of new bone formation had occurred by 3 weeks. The calcein label was mostly present in regions near the host bone surfaces (Figure 7a,b), but was also observed in isolated sites of osteoinductive bone formation more distant from the host bone. In the central regions of the
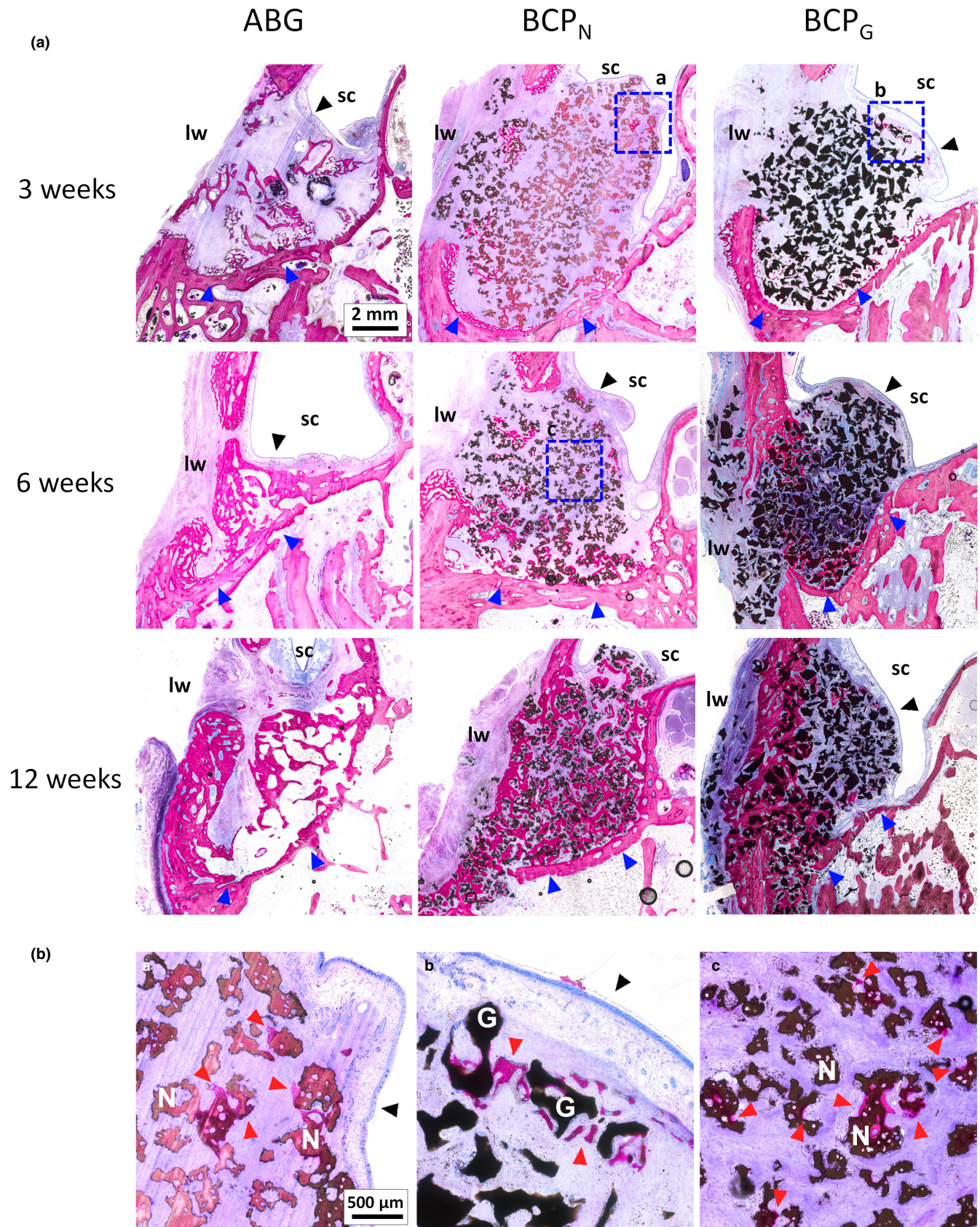
implants (Figure 7c,d), the labels XO (red, 6 weeks) and OTC (yellow, 9 weeks) were dominant, indicating that osteogenesis had mostly started there between week 3 and week 6. Evaluating the sequential deposition of the labels, the progression of bone formation with time could be clearly observed. Bone formation was observed to commonly originate at the surface of the calcium phosphate granules,

FIGURE 4 Histology of bone grafts implanted beneath the maxillary sinus floor (basic fuchsin-methylene blue). (a) Representative sections of ABG, BCP$_N$ and BCP$_G$ at time-points 3, 6 and 12 weeks are presented. ABG particles and calcium phosphate granules can be observed in direct contact with the bony sinus floor under the elevated Schneiderian membrane. Progressive bone formation and graft consolidation with time is evident. (b) Regions of bone formation observed in BCP$_N$ and BCP$_G$ near the Schneiderian membrane, are shown in higher magnification (blue dashed frames a-c, panel A). *pink*: bone matrix, *black/brown*: calcium phosphate granules, *sc*: sinus cavity, *lw*: lateral window, *black arrowheads*: Schneiderian membrane, *blue arrowheads*: sinus floor, *red arrowheads*: osteoinductive bone formation, *N*: BCP$_N$, *G*: BCP$_G$.

FIGURE 5 High magnification histology (basic fuchsin-methylene blue). Representative sections of BCP$_N$ (a, c, e, g) and BCP$_G$ (b, d, f, h) are presented at 3 weeks (a, b), 6 weeks (c, d) and 12 weeks (e, f) post-surgery. Bone matrix is observed between and in direct contact with calcium phosphate granules. Maturation of bone tissue over time can be appreciated, with early bone characterized by woven bone morphology and sites of osteoid deposition, while mature bone is characterized by lamellar phenotype. Aligned, cuboidal osteoblasts and osteocytes can be observed at all time-points. Active phagocytosis of calcium phosphate material by large multinucleated cells was observed at all timepoints (g, h). *B*: bone, *O*: osteoid, *C*: capillary, *black arrowheads*: osteoblasts, *white arrowheads*: phagocytosing multinucleated cells, yellow arrowheads: osteocytes.
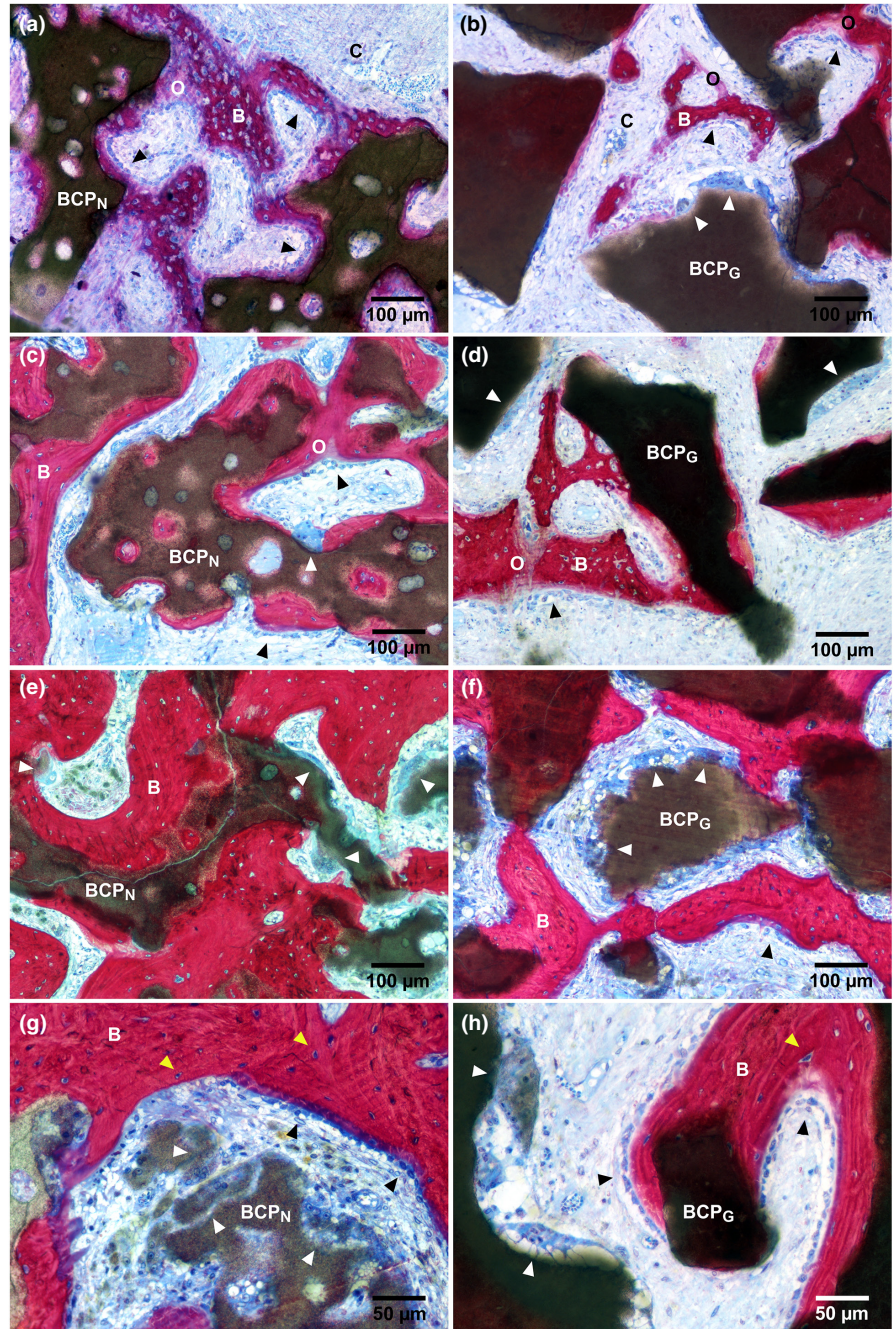
with the fluorochrome label CN in regions near host bone and XO in the core of the implants, being deposited directly against BCP$_N$ and BCP$_G$. OTC was less frequently observed in direct contact with the calcium phosphate surface, indicating that most granules were already incorporated into the mineralized bone matrix between 6 and 9 weeks.

3.2 | Clinical MSFA study

3.2.1 | Participants, treatment and baseline data

A total of 10 participants were enrolled in the trial, of whom five were allocated to the ABG group and five to the BCP$_N$ group. The
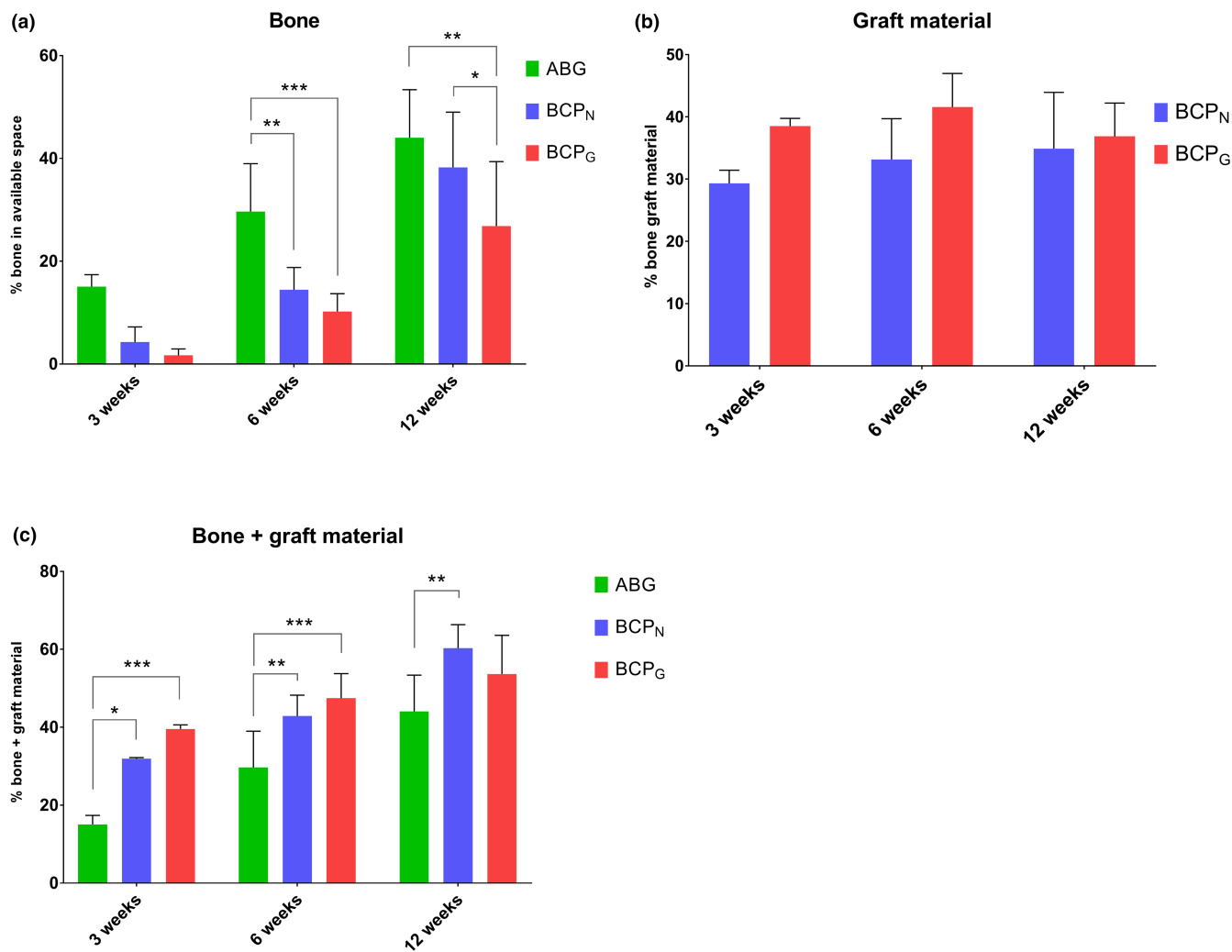
(a)

(b)

(c)

FIGURE 6 Histomorphometry of graft tissue. (a) Percentage of bone matrix in available space for ABG, BCP_N and BCP_G. (b) Percentage of residual graft material for calcium phosphate bone graft substitutes BCPN and BCPG. (c) Percentage of bone and graft material in graft tissue for ABG, BCP_N and BCP_G.

Sociodemographic and treatment information of the patient cohort is presented in Table 1. Participants in the two treatment arms were not significantly different in age and gender. Likewise, there were no significant differences between the treatment characteristics of the cohorts, including unilateral or bilateral MSFA, number of implants per patient, and implant dimensions. Residual vertical bone height in the atrophic posterior maxilla was similar for both treatment groups. Except for one participant in the BCP_N group who missed the final visit at 17 months, all patients completed follow-up.

3.2.2 | Implant stability

The results of implant stability measurements are presented in Table 2. Although the mean ISQ was higher for BCP_N in all instances, there were no significant differences between the treatment groups in primary or secondary stability on either the bucco-lingual and the mesio-distal axes. Similarly, no significant differences were determined for ΔISQ. Mean ΔISQ values were close to zero for both

treatment groups, indicating a minimal difference between primary and secondary implant stability overall.

3.2.3 | Bone height

Bone height was not significantly different between the ABG and BCP_N groups during the entire study follow-up (Figure 8). For both treatment groups, bone height after the MSFA procedure was significantly greater versus baseline, indicating successful sinus floor augmentation. After MSFA, a trend of decreasing bone height was apparent over time for both groups, albeit only significant for ABG at 11 and 17 months.

3.2.4 | New bone formation

The histology of trephine core biopsies was used to evaluate new bone formation in the augmented maxillary sinus floor. Low

FIGURE 7 Histology of fluorochrome labels. Calcium-binding fluorochrome labels CN (3 weeks, green), XO (red, 6 weeks) and OTC (yellow, 9 weeks) indicate sites of active bone matrix mineralization at the respective time-points. Representative sections of BCP_N (a, c, e,) and BCP_G (b, d, f) are shown from regions nearby host bone (a, b) and from the center of the grafts (c, d). Sequential deposition of the labels shows that bone formation originated against the surface of the graft materials and progressed outwards (e, f).
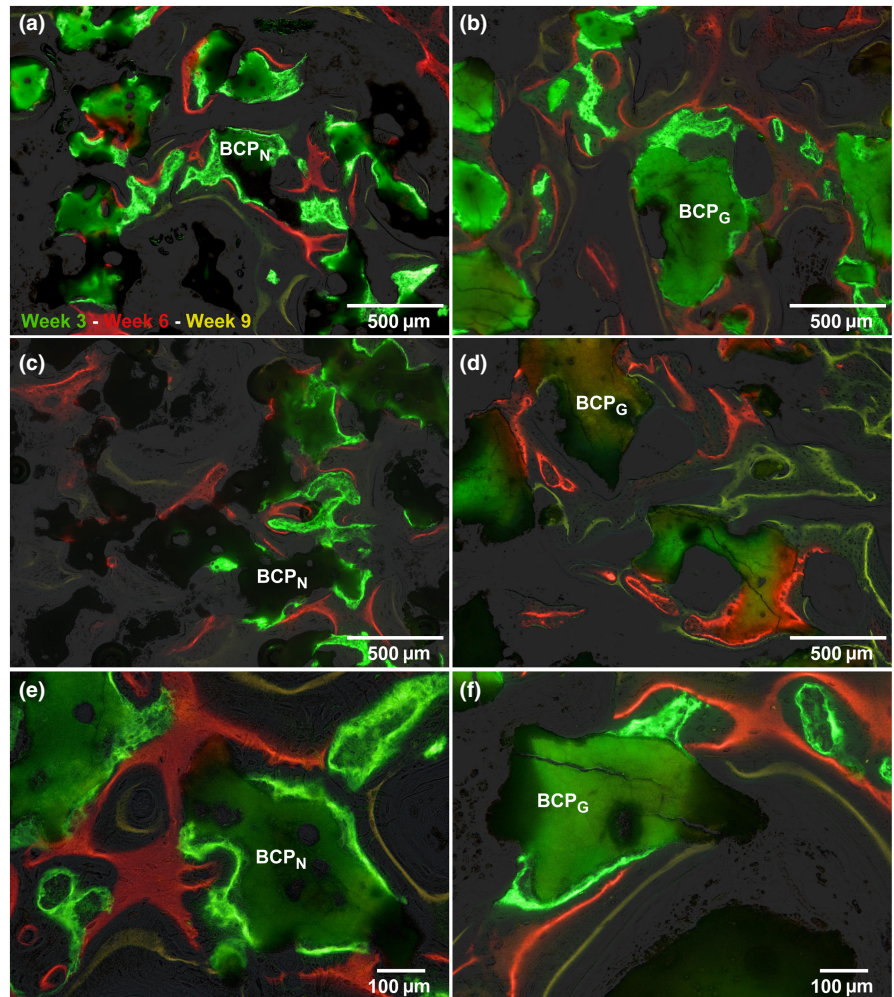
magnification histological overviews (Figure 9) revealed new bone formation throughout the biopsies for both ABG and BCPN, whereas BCPN specimens presented residual calcium phosphate particles. ABG biopsies appeared to have a slightly greater soft tissue component than BCP_N biopsies. On higher magnification (Figure 9), BCP_N biopsies demonstrated direct apposition of bone tissue against the calcium phosphate particles, and bone tissue was bridging between particles (Figure 9a,b). Bone tissue had a normal appearance and presented osteocytes in lacunae (Figure 9c). New bone formation was observed originating at the surface of the BCP_N particles (Figure 9e).

Histomorphometry of the graft area in the biopsies (Figure 9f,g) revealed a comparable area percentage of bone tissue in the available space for BCP_N (45.7 ± 23.0%) and ABG (43.4 ± 13.6%) (Figure 9f). The area percentages of combined bone and residual graft material were also comparable, although the difference between the means of BCP_N (60.9 ± 17.5%) and ABG (43.4 ± 13.6%) was greater (Figure 9g).

3.2.5 | Clinical outcomes

Table 3 presents the clinical outcomes of participants treated with ABG and BCP_N. First of all, both treatment groups exhibited 100%

implant survival during the study follow-up. Among the reported adverse events related to the MSFA procedure were two cases of maxillary sinusitis in the BCP_N group and one case of vestibular infection in the ABG group. The incidence of adverse events was not significantly different between the treatment groups. Similarly, no significant differences between the treatment groups were detected for the incidence of Schneiderian membrane perforations and implant apex protrusions. With regard to implant health scores, gingival index and plaque index were primarily graded "0" and "1" in both treatment groups, with no significant difference between groups. However, a significant difference was recorded for the bleeding index, with a higher incidence of gingival bleeding in the BCP_N group compared to the ABG. Implant probing depth was comparable for both treatment groups. Reported pain by visual analog scale (0–10) was comparable between the treatment groups and was below 1 for >90% of measurements without an apparent trend over time (data not shown).

4 | DISCUSSION

The current study describes the preclinical and clinical evaluation of osteoinductive calcium phosphate with submicron surface

TABLE 1 Participants, treatment, and baseline data.

	Total	ABG	BCP$_N$	p-value[a]
Participants n	10	5	5	
Age (years) Mean (SD), [min-max], [CI 95%]	56.7 (11.2) [33–74]	55.8 (14.7) [33–74] [37.5–74.1]	57.6 (9.7) [46–72] [45.6–69.6]	.794
Gender n (%)				
Female	3 (30)	2 (40)	1 (20)	>.999
Male	7 (70)	3 (60)	4 (80)	
MSFA procedure n (%)				
Unilateral	4 (40)	1 (20)	3 (60)	>.999
Bilateral	6 (60)	4 (80)	2 (40)	
Residual bone height (mm) Mean (SD), [min-max], [CI 95%]	3.1 (1.1) [2.0–5.8]	3.4 (1.3) [2.0–5.8] [2.39–4.44]	2.6 (0.8) [2.0–4.0] [1.88–3.38]	.323
Number of implants n (%)	23 (100)	12 (52.2)	11 (47.8)	
Implants per patient Mean (SD), [min-max], [CI 95%]	2.4 (1.6) [1–6]	2.4 (1.1) [1–4] [0.98–3.82]	2.2 (2.2) [1–6] [−0.49–4.89]	.476
Implant size (mm) Mean (SD), [min-max], [CI 95%]				
Diameter	4.2 (3.7) [3.6–4.8]	4.2 (3.1) [3.6–4.8] [3.95–4.35]	4.4 (4.5) [3.6–4.8] [3.95–4.79]	.175
Length	10.3 (1.3) [8.0–13.0]	10.4 (1.0) [9.0–11.2] [9.72–11.0]	10.3 (1.7) [8.0–13.0] [8.71–11.9]	.783

[a]Mann–Whitney U test or Fisher's exact test.

TABLE 2 Implant stability.

|	Bucco-lingual			Mesio-distal		
	ABG	BCP$_N$	p-value[a]	ABG	BCP$_N$	p-value[a]
ISQ T0 (Primary stability) Mean (SD), [min-max]	57.0 (12.3) [43.0–79.0]	60.2 (17.7) [30.0–79.0]	.820	61.9 (12.44) [43.7–79.0]	67.0 (13.0) [45.6–80.0]	.657
ISQ T1 (Secondary stability, 6 months) Mean (SD), [min-max]	56.1 (10.4) [43.0–71.0]	65.4 (10.7) [53.7–83.0]	.306	59.6 (13.1) [42.3–77.0]	70.7 (17.1) [43.0–98.0]	.2269
Δ ISQ (T1-T0) Mean (SD), [min-max]	−0.8 (10.6) [−21.0–16.7]	1.1 (12.1) [−21.0–10.7]	.820	−2.3 (12.3) [−30.7–13.0]	−0.8 (11.6) [−13.3–18.0]	.822

[a]Two-way ANOVA, Holm-Sidak's multiple comparisons test.

topography as a bone graft substitute for MSFA. In a preclinical sheep model, two biphasic calcium phosphates with needle-shaped and grain-shaped submicron surface topography were compared with autograft as the control. After MSFA, vertical augmentation height was greater for both synthetic materials versus ABG at all time-points. Both BCP$_N$ and BCP$_G$ were biocompatible, supporting bony ingrowth with direct bone apposition against the materials, while resorbing at a comparable rate. Both BCP$_N$ and BCP$_G$ exhibited osteoinductive bone formation as early as 3 weeks post-implantation, but BCP$_N$ demonstrated significantly more bone formation than BCP$_G$ at

the study endpoint of 12 weeks. Only BCP$_N$ reached an equivalent amount of bone formation in the available space and a greater proportion of calcified material (bone + graft material) beneath the maxillary sinus floor compared to the clinical "gold standard" ABG, after 12 weeks. These results were validated in a clinical study, in which BCP$_N$ was compared to autograft in a cohort of 10 patients receiving lateral window MSFA with two-stage implant placement. In this small study population, BCP$_N$ was found to be comparable to ABG in implant stability, bone height, new bone formation in trephine core biopsies, and the majority of clinical outcomes.

FIGURE 8 Bone height in the posterior maxilla as measured by CT at the location of the implants at baseline, month 5, 11 and 17 months. Green asterisks indicate significance between timepoints for ABG, blue asterisks indicate significance between timepoints for BCP_N. No significant differences were determined between the treatment groups.
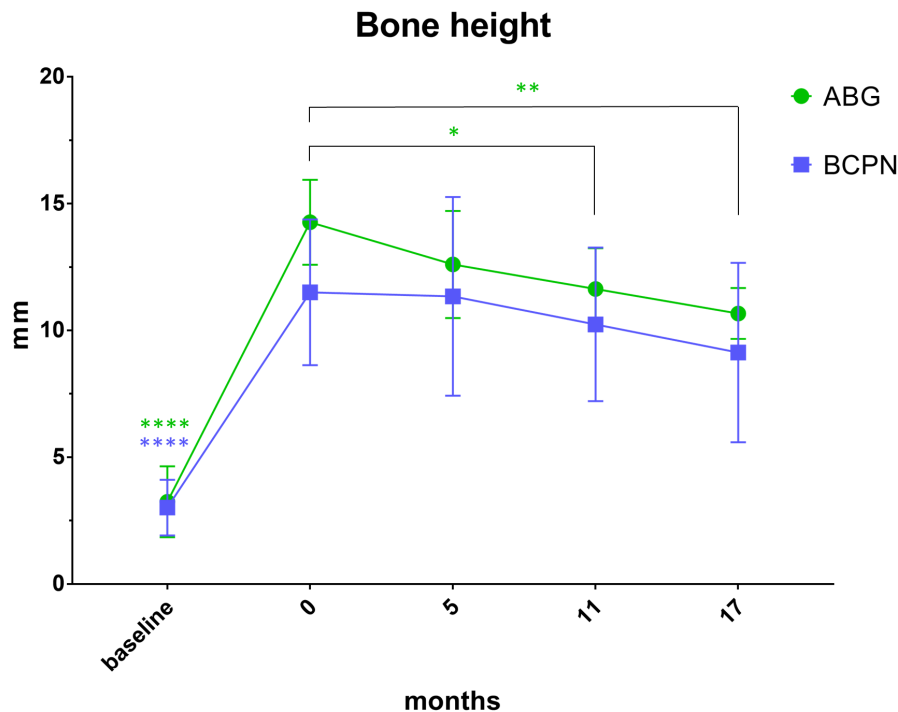
In recent years, there has been an increasing interest in the effect of biomaterial surface topographies on biological responses, with the goal of optimizing favorable healing responses following implantation. While relationships have been determined between topography and osteogenic differentiation of stem cells (Dobbenga et al., 2016; Gui et al., 2018; Huang et al., 2019), other research has focused on immunomodulatory effects (Luu et al., 2015; Yang et al., 2019). The osteoinductive potential of calcium phosphates has been reproducibly linked to the presence of a submicron surface topography, that is, a topography of surface crystals smaller than 1 μm in diameter (Duan et al., 2016; Duan et al., 2019; Duan, Barbieri, De Groot, et al., 2018; Duan, Barbieri, Luo, et al., 2018; Yuan et al., 2010). Recent studies have suggested that upregulation of anti-inflammatory M2 macrophages and osteoclastogenesis play an additional role in osteoinduction by calcium phosphate with submicron topography (Chen et al., 2020; Davison et al., 2014, 2015; Li et al., 2020). Further research is needed to elucidate how surface crystal morphology influences bone regeneration by calcium phosphate bone graft substitutes. A recent comprehensive review by Bohner and Miron proposed a new mechanism for intrinsic osteoinduction by biomaterials, introducing a novel concept of calcium and/or phosphate depletion that could form the trigger for osteoinduction. This mechanism takes into account the composition, volume, and architecture of materials, as well as the potential roles of macrophages and osteoclasts (Bohner & Miron, 2019).

Both bone graft substitutes that were studied in the sheep model, BCP_N and BCP_G, have a submicron topography and were previously demonstrated to possess osteoinductive capacity in ectopic implantation models (Duan et al., 2019; Duan, Barbieri, Luo, et al., 2018; Le Nihouannen et al., 2005). Interestingly, when evaluated in the same

canine intramuscular implantation model by our group, osteoinductive bone formation was determined in 100% of implants for both BCP_N and BCP_G, but the area percentage of bone as determined by histomorphometry was approximately 10x greater for BCP_N (24.5% ± 4.3 vs. 2.4% ± 1.4%) (Duan et al., 2019; Duan, Barbieri, Luo, et al., 2018). This suggests that BCP_N has a higher intrinsic osteoinductive potential than BCP_G. Due to its biphasic composition (30% HA, 70% TCP) and novel submicron needle-shaped topography, BCP_N (MagnetOs, Kuros Biosciences BV) is different from an earlier commercial bone graft manufactured by our group for dental applications (Vivoss/Osopia, Regedent AG). This earlier material has a larger component of TCP (<10% HA/>90% TCP) and a submicron grain-shaped surface topography and may be associated with faster resorption properties.

A potential explanation for the difference in bone forming potential of BCP_N and BCP_G in both the current orthotopic model and the ectopic implantation model mentioned above may lie in their surface crystal morphology. While BCP_N and BCP_G overall have similar physicochemical properties (Appendix, Table S1), including granule size, HA/ßTCP phase composition, and porosity, the materials are different in the morphology of their submicron surface crystals. In a recent study by our group, osteoinduction by calcium phosphates with different morphologies of submicron surface crystals was evaluated (Duan et al., 2019). A material with needle-shaped topography showed accelerated osteoinductive bone formation versus a material with grain-shaped topography (Duan et al., 2019). These results indicated that, besides the dimension of the surface features (i.e., submicron vs. micron), the morphology of surface crystals also affects osteoinductive capacity. In the current study, the needle-shaped submicron topography of BCP_N was similarly associated with a higher bone-forming potential than BCP_G.
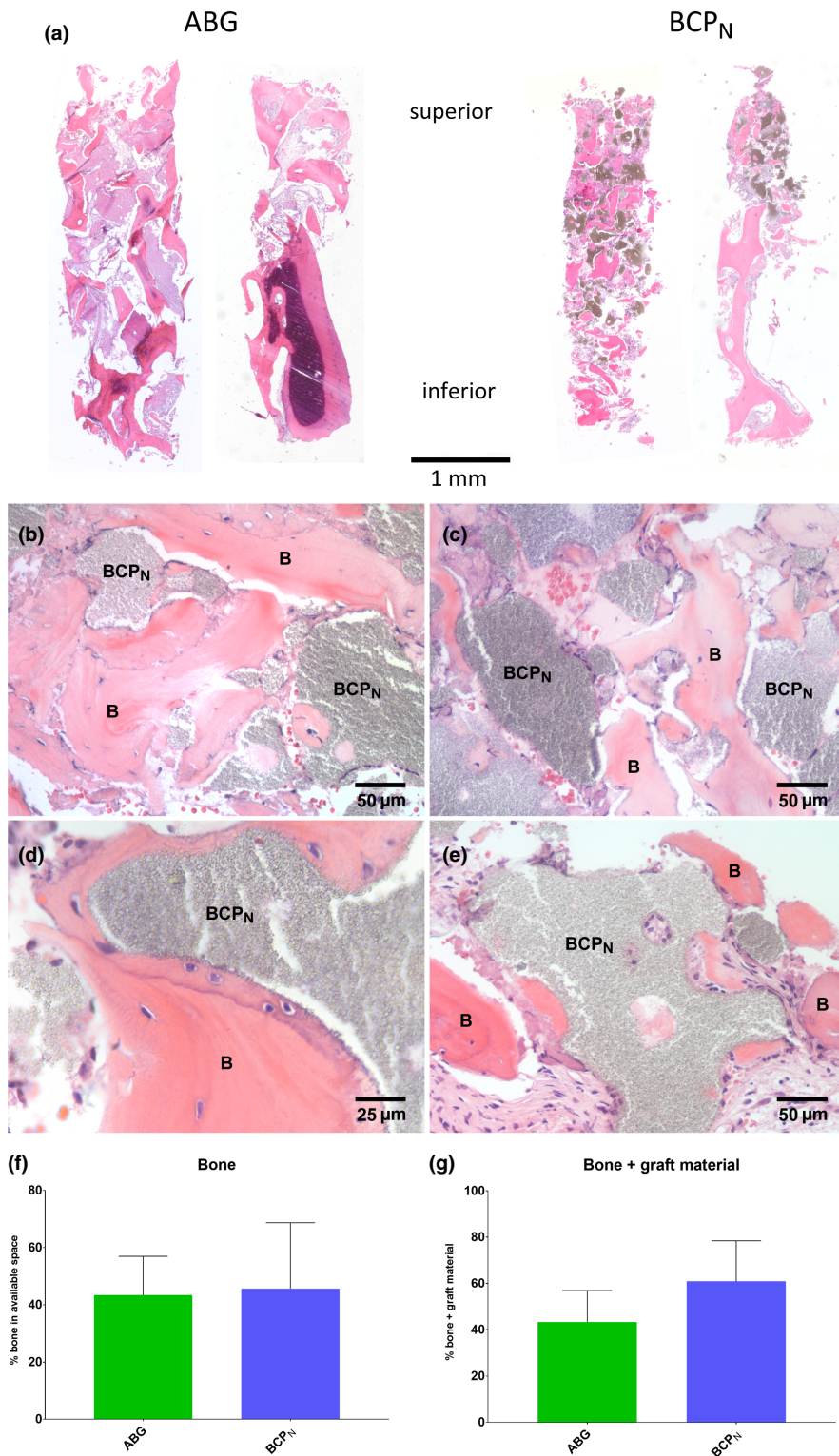
FIGURE 9 Histology and histomorphometry of clinical trephine core biopsies. (a) Representative histological micrographs of biopsies (hematoxylin–eosin) of ABG and BCP$_N$. In the inferior aspect, the original dense alveolar bone of the sinus floor can be occasionally observed. The dark granular material in the BCP$_N$ specimens represents the BCP$_N$ granules. (b–e) High magnification histology of trephine core biopsies of the BCP$_N$ group (hematoxylin–eosin). Direct bone apposition against BCP$_N$ granules is apparent, with bone matrix engulfing BCP$_N$ granules (b–d). New bone formation is occasionally observed originating at the surface and inside pores of the granules (e). (f, g) Histomorphometry of clinical trephine core biopsies. (f) Percentage of bone matrix in available space for ABG and BCP$_N$. (g) Percentage of bone and graft material trephine cores. No significant differences were determined between ABG and BCP$_N$.

To our knowledge, the observed early bone formation in synthetic implants in the space created after maxillary sinus floor elevation, distant from the host bone and near the Schneiderian membrane, has not been previously reported. Although studies have suggested that the Schneiderian membrane itself has osteoinductive potential (Srouji et al., 2010), this concept has been invalidated in later studies (Jungner et al., 2015; Scala et al., 2012). However, the Schneiderian membrane has been shown to be osteogenic, since it harbors a niche of mesenchymal osteoprogenitor cells (Berbéri et al., 2017; Graziano et al., 2012; Gruber et al., 2004; Li et al., 2015). Furthermore, mucosal epithelia such as the Schneiderian membrane are known to contain high numbers of immune cells, including macrophages, because they form a primary defense against invading pathogens (Oh et al., 2020; Russell et al., 2015). In light of earlier results that have

TABLE 3 Clinical outcomes.

		ABG	BCP$_N$	p-value[a]
Implant survival n/total (%)		12/12 (100)	11/11 (100)	>.999
Adverse events related to MSFA n (%)				
All		1 (20)	2 (40)	>.999
Sinusitis maxillaris		0 (0)	2 (40)	.444
Vestibular infection		1 (20)	0 (0)	>.999
Schneiderian membrane perforation n/total (%)		4/9 (44.4)	2/7 (28.6)	.633
Implant apex protrusion n/total (%)		3/12 (25)	3/11 (27.3)	>.999
Implant health scores n				
Gingival index (0–3)	0	7	3	.243
	1	3	5	
	2	0	1	
	3	0	0	
Plaque index (0–3)	0	8	5	.443
	1	2	3	
	2	0	1	
	3	0	0	
Bleeding index (0–2)	0	8	1	.006
	1	2	8	
Probing depth (mm) Mean (SD), [min-max], [CI 95%]		2.2 (0.6) [1.8–3.8] [1.79–2.63]	2.8 (0.8) [1.6–3.8] [2.16–3.40]	.181

[a]Fisher–Freeman–Halton Exact test or Mann–Whitney U test.

suggested a role for macrophages in bone induction, it is possible that macrophages from the Schneiderian may have migrated to the nearby implanted bone grafts, and subsequently polarized to the pro-regenerative M2 phenotype. The observed early bone induction near the Schneiderian membrane may therefore have resulted from an interaction between the bone graft surface and macrophages and osteoprogenitor cells originating from the Schneiderian membrane.

The performance of BCP$_N$ demonstrated in the sheep model was clinically validated in a first clinical study in terms of functionality, that is, bone formation, volume augmentation, and implant stability. Bone formation as determined by histomorphometry of trephine core biopsies was equivalent for BCP$_N$ and the control ABG. Interestingly, the mean area percentages of bone in available space for BCP$_N$ and ABG in the sheep study were comparable to the values obtained in the clinical study, while mean area percentages of residual graft material and combined bone and graft material were also similar for BCP$_N$ between the two studies.

Vertical bone height after MSFA in the preclinical model was greater for the synthetic bone substitutes than ABG at all timepoints, which indicates that ABG had a lower volume stability than the synthetic grafts. However, in the clinical study, bone height was comparable between ABG and BCP$_N$ at all follow-up visits. The observation that ABG undergoes greater volume reductions than calcium phosphate-based bone graft substitutes has been often reported in the literature (Cosso et al., 2014; Jensen, Schou, Svendsen, et al., 2012; Lutz et al., 2015; Schlegel et al., 2003; Shanbhag et al., 2014). Because of concerns that ABG resorption might compromise MSFA, especially with two-stage implant placement, it has been recommended to use bone graft substitutes as an extender or substitute for ABG to maintain graft volume (Jensen, Schou, Stavropoulos, et al., 2012; Kühl et al., 2014; Mardinger et al., 2011). Long term graft volume stability is considered a favorable outcome in MSFA, although there is so far no evidence indicating that volume loss negatively affects implant placement or survival (Shanbhag et al., 2014). The advantage of using a BCP that has a moderate resorption rate is that it can provide initial stability to the new bone and allow the tissue to mature, while it is gradually remodeled and replaced by bone tissue over time. RFA has been used as a tool for the assessment of bone quality and osseointegration. Previous studies have indicated that good primary/mechanical stability, that is, lack of implant micromovement, is a prerequisite for proper peri-implant healing and osseointegration, which leads to secondary/biological stability (Monje et al., 2019). Several studies have positively correlated implant stability to bone quality, although other factors have been found to affect ISQ, including implant location, insertion torque, dimensions, and design of the implant (Huang et al., 2020). In our clinical study, RFA of dental implants revealed comparable primary and secondary implant stability for ABG and BCP$_N$, with a negligible difference between primary and secondary stability within groups.

It is challenging to compare the outcomes of the current work directly to results obtained in studies that have used conventional, non-osteoinductive bone graft substitutes. Many pre-clinical studies that have evaluated such materials lack a positive control, used different timepoints and assessment methods, or used bone substitutes in combination with autologous bone or other adjuncts (e.g., stem cells, platelet rich plasma, composite grafts) (Alayan et al., 2016; Barboni et al., 2013; Grageda et al., 2005; Gutwald et al., 2010; Klijn et al., 2012; Mangano et al., 2015; Philipp et al., 2014; Saffarzadeh et al., 2009; Sauerbier, Stricker, et al., 2010; Sauerbier, Stubbe, et al., 2010). However, in studies that evaluated bovine xenograft, porous HA, and demineralized freeze-dried bone allografts versus ABG in MSFA models, the authors advised against the use of these materials as standalone substitutes for ABG because they resulted in lower bone-implant contact (Haas, Baron, et al., 2002; Haas, Haidvogl, et al., 2002; Jensen et al., 2013). In other clinical MSFA studies, bone percentage in bone core biopsies was commonly higher for ABG compared to bone graft substitutes (Danesh-Sani et al., 2017; Handschel et al., 2009; Klijn et al., 2010a; Papageorgiou et al., 2016; Stumbras et al., 2019), while results of comparisons between synthetics, xenografts and allografts have been variable (Annibali et al., 2015; Kurkcu et al., 2012; Lindgren et al., 2009; Papageorgiou et al., 2016; Schmitt et al., 2013). Still, questions remain

on the relevance of bone substitute selection for MSFA, since clear influence of graft type on clinical outcomes and implant survival has so far not been reported (Al-Nawas & Schiegnitz, 2014; Del Fabbro et al., 2005; Nkenke & Stelzle, 2009; Starch-Jensen et al., 2018).

The strengths of this study include the thorough evaluation of bone formation by two similar synthetic bone graft substitutes with different surface crystal morphology, in a clinically relevant sheep model of MSFA, using the gold standard autograft as a control. Moreover, this study is translational because the pre-clinical results were clinically validated in a human trial that used a full range of assessment methods to compare a bone substitute to the gold standard. A limitation of the sheep MSFA model is that it involves the implantation of bone grafts into the sub-Schneiderian space in non-atrophic maxillae with intact molars, while clinical MSFA cases often involve augmentation of severely resorbed alveolar bone in edentate patients. Furthermore, we have not evaluated the placement and osseointegration of dental implants in the sheep model. The clinical study was limited by the relatively low number of patients that were enrolled. A larger sample size would have led to an increase in statistical power that may have resulted in the discovery of significant differences.

In conclusion, the present translational work demonstrated successful MSFA with a novel osteoinductive calcium phosphate with needle-shaped surface topography. In a sheep model of MSFA comparing two osteoinductive calcium phosphate bone substitutes with submicron topography, a material with a needle-shaped topography demonstrated enhanced bone formation versus a material with a grain-shaped topography. Moreover, the material with needle-shaped topography reached an equivalent amount of bone formation (in the available space) compared to the "gold standard" ABG. These results were validated in a small prospective clinical study, in which the same bone substitute reached comparable results to autograft on almost all outcomes. These findings confirm that morphology of submicron surface features on calcium phosphates dictates their in situ bone-forming potential. Osteoinductive BCP promoted the formation of mature bone in direct contact with the material, facilitating osseointegration and stability of dental implants after 1 year of placement while avoiding the disadvantages of autograft (i.e., second surgical site, graft resorption). Future investigation of osteoinductive calcium phosphates in larger clinical studies is recommended to further explore their potential as stand-alone bone graft substitute materials for maxillofacial surgery.

AUTHOR CONTRIBUTIONS

Lukas Alexander van Dijk: Conceptualization (equal); data curation (lead); formal analysis (lead); investigation (lead); methodology (lead); writing – original draft (lead). **Nard G. Janssen:** Conceptualization (equal); investigation (equal); methodology (equal); writing – review and editing (equal). **Florence van Barrère-de Groot:** Conceptualization (equal); funding acquisition (equal); methodology (equal); project administration (equal); supervision (equal); writing – review and editing (equal). **Joost D. de Bruijn:** Conceptualization (equal); funding acquisition (equal); methodology (equal); project administration (equal); supervision (equal); writing – review and editing (equal). **Debby Gawlitta:** Conceptualization (equal); funding acquisition (equal); investigation (equal); methodology (equal); project administration (equal); supervision (equal); writing – review and editing (equal). **Antoine J.W.P. Rosenberg:** Conceptualization (equal); funding acquisition (equal); investigation (equal); methodology (equal); project administration (equal); supervision (lead); writing – review and editing (equal).

ACKNOWLEDGMENTS

CONFLICT OF INTEREST

LvD, FdG, JdB are employees of Kuros Biosciences BV. JdB and FdG have patents issued on synthetic bone graft technology. JdB is stockholder of Kuros Biosciences BV. All other authors have no conflicts of interest to declare.

DATA AVAILABILITY STATEMENT

The data that support the findings of this study are available from the authors, upon reasonable request.

ORCID

Lukas A. van Dijk https://orcid.org/0000-0002-2018-4041
Nard G. Janssen https://orcid.org/0000-0002-0623-4559
Alessia Longoni https://orcid.org/0000-0002-9866-0263
Joost D. de Bruijn https://orcid.org/0000-0003-0367-3633
Debby Gawlitta https://orcid.org/0000-0001-9622-3062
Antoine J. W. P. Rosenberg https://orcid.org/0000-0002-0360-0576

REFERENCES

Alayan, J., Vaquette, C., Saifzadeh, S., Hutmacher, D., & Ivanovski, S. (2016). A histomorphometric assessment of collagen-stabilized anorganic bovine bone mineral in maxillary sinus augmentation - a randomized controlled trial in sheep. *Clinical Oral Implants Research*, *27*, 734–743.

Al-Nawas, B., & Schiegnitz, E. (2014). Augmentation procedures using bone substitute materials or autogenous bone - a systematic review and meta-analysis. *European Journal of Oral Implantology*, 7, S219–S234.

Annibali, S., Iezzi, G., Sfasciotti, G. L., Cristalli, M. P., Vozza, I., Mangano, C., La Monaca, G., & Polimeni, A. (2015). (2015) histological and histomorphometric human results of HA-Beta-TCP 30/70 compared to three different biomaterials in maxillary sinus augmentation at 6 months: A preliminary report. *BioMed Research International*, *2015*, 1–7.

Barboni, B., Mangano, C., Valbonetti, L., Marruchella, G., Berardinelli, P., Martelli, A., Muttini, A., Mauro, A., Bedini, R., Turriani, M., Pecci, R., Nardinocchi, D., Zizzari, V. L., Tetè, S., Piattelli, A., & Mattioli, M. (2013). Synthetic bone substitute engineered with amniotic epithelial cells enhances bone regeneration after maxillary sinus augmentation. *PLoS ONE*, *8*, e63256.

Barroso-Panella, A., Gargallo-Albiol, J., & Hérnandez-Alfaro, F. (2018). Evaluation of bone stability and esthetic results after immediate implant placement using a novel synthetic bone substitute in the anterior zone: Results after 12 months. *The International Journal of Periodontics & Restorative Dentistry*, 38, 235–243.

Berbéri, A., Al-Nemer, F., Hamade, E., Noujeim, Z., Badran, B., & Zibara, K. (2017). Mesenchymal stem cells with osteogenic potential in human maxillary sinus membrane: An in vitro study. *Clinical Oral Investigations*, 21, 1599–1609.

Bohner, M., & Miron, R. J. (2019). A proposed mechanism for material-induced heterotopic ossification. *Materials Today*, 22, 132–141.

Chen, X., Wang, M., Chen, F., Wang, J., Li, X., Liang, J., Fan, Y., Xiao, Y., & Zhang, X. (2020). Correlations between macrophage polarization and osteoinduction of porous calcium phosphate ceramics. *Acta Biomaterialia*, 103, 318–332.

Cosso, M. G., De Brito, R. B., Piattelli, A., Shibli, J. A., & Zenóbio, E. G. (2014). Volumetric dimensional changes of autogenous bone and the mixture of hydroxyapatite and autogenous bone graft in humans maxillary sinus augmentation. A multislice tomographic study. *Clinical Oral Implants Research*, 25, 1251–1256.

Danesh-Sani, S. A., Engebretson, S. P., & Janal, M. N. (2017). Histomorphometric results of different grafting materials and effect of healing time on bone maturation after sinus floor augmentation: A systematic review and meta-analysis. *Journal of Periodontal Research*, 52, 301–312.

Danesh-Sani, S. A., Loomer, P. M., & Wallace, S. S. (2016). A comprehensive clinical review of maxillary sinus floor elevation: Anatomy, techniques, biomaterials and complications. *British Journal of Oral and Maxillofacial Surgery*, 54, 724–730.

Davison, N. L., Gamblin, A. L., Layrolle, P., Yuan, H., de Bruijn, J. D., & Barrère-de Groot, F. (2014). Liposomal clodronate inhibition of osteoclastogenesis and osteoinduction by submicrostructured beta-tricalcium phosphate. *Biomaterials*, 35, 5088–5097.

Davison, N. L., Su, J., Yuan, H., van den Beucken, J. J. J. P., de Bruijn, J. D., & de Groot, F. B. (2015). Influence of surface microstructure and chemistry on osteoinduction and osteoclastogenesis by biphasic calcium phosphate discs. *European Cells and Materials*, 29, 314–329.

De Ruiter, A., Janssen, N., Van Es, R., Frank, M., Meijer, G., Koole, R., & Rosenberg, T. (2015). Micro-structured beta-tricalcium phosphate for repair of the alveolar cleft in cleft lip and palate patients: A pilot study. *Cleft Palate-Craniofacial Journal*, 52, 336–340.

Del Fabbro, M., Testori, T., Francetti, L., & Weinstein, R. (2005). Systematic review of survival rates for implants placed in the grafted maxillary sinus. *The Journal of Prosthetic Dentistry*, 94, 266.

Dobbenga, S., Fratila-Apachitei, L. E., & Zadpoor, A. A. (2016). Nanopattern-induced osteogenic differentiation of stem cells—A systematic review. *Acta Biomaterialia*, 46, 3–14.

Duan, R., Barbieri, D., De Groot, F., De Bruijn, J. D., & Yuan, H. (2018). Modulating bone regeneration in rabbit condyle defects with three surface-structured tricalcium phosphate ceramics. *ACS Biomaterials Science and Engineering*, 4, 3347–3355.

Duan, R., Barbieri, D., Luo, X., Weng, J., Bao, C., De Bruijn, J. D., & Yuan, H. (2018). Variation of the bone forming ability with the physicochemical properties of calcium phosphate bone substitutes. *Biomaterials Science*, 6, 136–145.

Duan, R., Barbieri, D., Luo, X., Weng, J., de Bruijn, J. D., & Yuan, H. (2016). Submicron-surface structured tricalcium phosphate ceramic enhances the bone regeneration in canine spine environment. *Journal of Orthopaedic Research*, 34, 1865–1873.

Duan, R., van Dijk, L. A., Barbieri, D., de Groot, F., Yuan, H., & de Bruijn, J. D. (2019). Accelerated bone formation by biphasic calcium phosphate with a novel sub-micron surface topography. *European Cells & Materials*, 37, 60–73.

Emeka, N., & Neukam, F. W. (2014). Autogenous bone harvesting and grafting in advanced jaw resorption: Morbidity, resorption and implant survival. *European Journal of Oral Implantology*, 7, S203–S217.

Gjerde, C. G., Shanbhag, S., Neppelberg, E., Mustafa, K., & Gjengedal, H. (2020). Patient experience following iliac crest-derived alveolar bone grafting and implant placement. *International Journal of Implant Dentistry*, 6, 4.

Grageda, E., Lozada, J. L., Boyne, P. J., Caplanis, N., & McMillan, P. J. (2005). Bone formation in the maxillary sinus by using platelet-rich plasma: An experimental study in sheep. *The Journal of Oral Implantology*, 31, 2–17.

Graziano, A., Benedetti, L., Massei, G., Cusella de Angelis, M. G., Ferrarotti, F., & Aimetti, M. (2012). Bone production by human maxillary sinus mucosa cells. *Journal of Cellular Physiology*, 227, 3278–3281.

Gruber, R., Kandler, B., Fuerst, G., Fischer, M. B., & Watzek, G. (2004). Porcine sinus mucosa holds cells that respond to bone morphogenetic protein (BMP)-6 and BMP-7 with increased osteogenic differentiation in vitro. *Clinical Oral Implants Research*, 15, 575–580.

Gui, N., Xu, W., Myers, D. E., Shukla, R., Tang, H. P., & Qian, M. (2018). The effect of ordered and partially ordered surface topography on bone cell responses: A review. *Biomaterials Science*, 6, 250–264.

Gutwald, R., Haberstroh, J., Kuschnierz, J., Kister, C., Lysek, D. A., Maglione, M., Xavier, S. P., Oshima, T., Schmelzeisen, R., & Sauerbier, S. (2010). Mesenchymal stem cells and inorganic bovine bone mineral in sinus augmentation: Comparison with augmentation by autologous bone in adult sheep. *British Journal of Oral and Maxillofacial Surgery*, 48, 285–290.

Haas, R., Baron, M., Donath, K., Zechner, W., & Watzek, G. (2002). Porous hydroxyapatite for grafting the maxillary sinus: A comparative histomorphometric study in sheep. *The International Journal of Oral & Maxillofacial Implants*, 17, 337–346.

Haas, R., Haidvogl, D., Donath, K., & Watzek, G. (2002). Freeze-dried homogeneous and heterogeneous bone for sinus augmentation in sheep part I: Histological findings. *Clinical Oral Implants Research*, 13, 396–404.

Habibovic, P., Yuan, H., van den Doel, M., Sees, T. M., van Blitterswijk, C. A., & de Groot, K. (2006). Relevance of osteoinductive biomaterials in critical-sized orthotopic defect. *Journal of Orthopaedic Research*, 24, 867–876.

Handschel, J., Simonowska, M., Naujoks, C., Depprich, R. A., Ommerborn, M. A., Meyer, U., & Kübler, N. R. (2009). A histomorphometric meta-analysis of sinus elevation with various grafting materials. *Head and Face Medicine*, 5, 1–10.

Haugen, H. J., Lyngstadaas, S. P., Rossi, F., & Perale, G. (2019). Bone grafts: Which is the ideal biomaterial? *Journal of Clinical Periodontology*, 46, 92–102.

Hoekstra, J. W. M., Klijn, R. J., Meijer, G. J., van den Beucken, J. J. J. P., & Jansen, J. A. (2013). Maxillary sinus floor augmentation with injectable calcium phosphate cements: A pre-clinical study in sheep. *Clinical Oral Implants Research*, 24, 210–216.

Huang, H., Wu, G., & Hunziker, E. (2020). The clinical significance of implant stability quotient (ISQ) measurements: A literature review. *Journal of Oral Biology and Craniofacial Research*, 10, 629–638.

Huang, J., Chen, Y., Tang, C., Fei, Y., Wu, H., Ruan, D., Paul, M. E., Chen, X., Yin, Z., Heng, B. C., Chen, W., & Shen, W. (2019). The relationship between substrate topography and stem cell differentiation in the musculoskeletal system. *Cellular and Molecular Life Sciences*, 76, 505–521.

Janssen, N. G., Schreurs, R., de Ruiter, A. P., Sylvester-Jensen, H. C., Blindheim, G., Meijer, G. J., Koole, R., & Vindenes, H. (2019). Microstructured beta-tricalcium phosphate for alveolar cleft repair: A two-Centre study. *International Journal of Oral and Maxillofacial Surgery*, 48, 708–711.

Jensen, T., Schou, S., Gundersen, H. J. G., Forman, J. L., Terheyden, H., & Holmstrup, P. (2013). Bone-to-implant contact after maxillary sinus floor augmentation with bio-Oss and autogenous bone in different ratios in mini pigs. *Clinical Oral Implants Research*, *24*, 635–644.

Jensen, T., Schou, S., Stavropoulos, A., Terheyden, H., & Holmstrup, P. (2012). Maxillary sinus floor augmentation\with bio-Oss or bio-Oss mixed with autogenous bone as graft: A systematic review. *Clinical Oral Implants Research*, *23*, 263–273.

Jensen, T., Schou, S., Svendsen, P. A., Forman, J. L., Gundersen, H. J. G., Terheyden, H., & Holmstrup, P. (2012). Volumetric changes of the graft after maxillary sinus floor augmentation with bio-Oss and autogenous bone in different ratios: A radiographic study in minipigs. *Clinical Oral Implants Research*, *23*, 902–910.

Johansson, B., Grepe, A., Wannfors, K., & Hirsch, J. M. (2001). A clinical study of changes in the volume of bone grafts in the atrophic maxilla. *Dentomaxillofacial Radiology*, *30*, 157–161.

Jungner, M., Cricchio, G., Salata, L. A., Sennerby, L., Lundqvist, C., Hultcrantz, M., & Lundgren, S. (2015). On the early mechanisms of bone formation after maxillary sinus membrane elevation: An experimental histological and immunohistochemical study. *Clinical Implant Dentistry and Related Research*, *17*, 1092–1102.

Klijn, R. J., Hoekstra, J. W. M., Van Den Beucken, J. J. J. P., Meijer, G. J., & Jansen, J. A. (2012). Maxillary sinus augmentation with microstructured tricalcium phosphate ceramic in sheep. *Clinical Oral Implants Research*, *23*, 274–280.

Klijn, R. J., Meijer, G. J., Bronkhorst, E. M., & Jansen, J. A. (2010a). A meta-analysis of histomorphometric results and graft healing time of various biomaterials compared to autologous bone used as sinus floor augmentation material in humans. *Tissue Engineering - Part B: Reviews*, *16*, 493–507.

Klijn, R. J., Meijer, G. J., Bronkhorst, E. M., & Jansen, J. A. (2010b). Sinus floor augmentation surgery using autologous bone grafts from various donor sites: A meta-analysis of the total bone volume. *Tissue Engineering - Part B: Reviews*, *16*, 295–303.

Kühl, S., Payer, M., Kirmeier, R., Wildburger, A., Wegscheider, W., & Jakse, N. (2014). The influence of bone marrow aspirates and concentrates on the early volume stability of maxillary sinus grafts with deproteinized bovine bone mineral - first results of a RCT. *Clinical Oral Implants Research*, *25*, 221–225.

Kurkcu, M., Benlidayi, M. E., Cam, B., & Sertdemir, Y. (2012). Anorganic bovine-derived hydroxyapatite vs b-tricalcium phosphate in sinus augmentation: A comparative histomorphometric study. *Journal of Oral Implantology*, *38*, 519–526.

Le Nihouannen, D., Daculsi, G., Saffarzadeh, A., Gauthier, O., Delplace, S., Pilet, P., & Layrolle, P. (2005). Ectopic bone formation by microporous calcium phosphate ceramic particles in sheep muscles. *Bone*, *36*, 1086–1093.

Li, M., Guo, X., Qi, W., Wu, Z., De Bruijn, J. D., Xiao, Y., Bao, C., & Yuan, H. (2020). Macrophage polarization plays roles in bone formation instructed by calcium phosphate ceramics. *Journal of Materials Chemistry B*, *8*, 1863–1877.

Li, X., Rong, Q., & Chen, S. L. (2015). The innate osteogenic potential of the canine maxillary sinus membrane: An in vitro and in vivo study. *Journal of Biomaterials and Tissue Engineering*, *5*, 445–451.

Lindgren, C., Sennerby, L., Mordenfeld, A., & Hallman, M. (2009). Clinical histology of microimplants placed in two different biomaterials. *The International Journal of Oral & Maxillofacial Implants*, *24*, 1093–1100.

Löe, H., & Silness, J. (1963). Periodontal disease in pregnancy I. Prevalence and Severity. *Acta Odontologica Scandinavica*, *21*, 533–551.

Lutz, R., Berger-Fink, S., Stockmann, P., Neukam, F. W., & Schlegel, K. A. (2015). Sinus floor augmentation with autogenous bone vs. a bovine-derived xenograft - a 5-year retrospective study. *Clinical Oral Implants Research*, *26*, 644–648.

Luu, T. U., Gott, S. C., Woo, B. W. K., Rao, M. P., & Liu, W. F. (2015). Micro- and nanopatterned topographical cues for regulating macrophage

cell shape and phenotype. *ACS Applied Materials and Interfaces*, *7*, 28665–28672.

Mangano, C., Barboni, B., Valbonetti, L., Berardinelli, P., Martelli, A., Muttini, A., Bedini, R., Tetè, S., Piattelli, A., & Mattioli, M. (2015). In vivo behavior of a custom-made 3D synthetic bone substitute in sinus augmentation procedures in sheep. *Journal of Oral Implantology*, *41*, 241–251.

Mardinger, O., Chaushu, G., Sigalov, S., Herzberg, R., Shlomi, B., & Schwartz-Arad, D. (2011). Factors affecting changes in sinus graft height between and above the placed implants. *Oral Surgery, Oral Medicine, Oral Pathology, Oral Radiology and Endodontology*, *111*, e6–11.

Monje, A., Ravidà, A., Wang, H.-L., Helms, J. A., & Brunski, J. B. (2019). Relationship between primary/mechanical and secondary/biological implant stability. *The International Journal of Oral & Maxillofacial Implants*, *34*, s7–s23.

Nkenke, E., & Stelzle, F. (2009). Clinical outcomes of sinus floor augmentation for implant placement using autogenous bone or bone substitutes: A systematic review. *Clinical Oral Implants Research*, *20*, 124–133.

Oh, D., Xie, J., Vanderheijden, N., & Nauwynck, H. J. (2020). Isolation and characterization of a new population of nasal surface macrophages and their susceptibility to PRRSV-1 subtype 1 (LV) and subtype 3 (Lena). *Veterinary Research*, *51*, 1–15.

Papageorgiou, S. N., Papageorgiou, P. N., Deschner, J., & Götz, W. (2016). Comparative effectiveness of natural and synthetic bone grafts in oral and maxillofacial surgery prior to insertion of dental implants: Systematic review and network meta-analysis of parallel and cluster randomized controlled trials. *Journal of Dentistry*, *48*, 1–8.

Philipp, A., Duncan, W., Roos, M., Hämmerle, C. H., Attin, T., & Schmidlin, P. R. (2014). Comparison of SLA® or SLActive® implants placed in the maxillary sinus with or without synthetic bone graft materials - an animal study in sheep. *Clinical Oral Implants Research*, *25*, 1142–1148.

Raghoebar, G. M., Onclin, P., Boven, G. C., Vissink, A., & Meijer, H. J. A. (2019). Long-term effectiveness of maxillary sinus floor augmentation: A systematic review and meta-analysis. *Journal of Clinical Periodontology*, *46*, 307–318.

Roberts, T. T., & Rosenbaum, A. J. (2012). Bone grafts, bone substitutes and orthobiologics the bridge between basic science and clinical advancements in fracture healing. *Organogenesis*, *8*, 114–124.

Lenth Russ (2006) *Java applets for power and sample size*. 1–6.

Russell, M. W., Mestecky, J., Strober, W., Lambrecht, B. N., Kelsall, B. L., & Cheroutre, H. (2015). Overview: The mucosal immune system. *Mucosal Immunology: Fourth Edition*, *1–2*, 3–8.

Saffarzadeh, A., Gauthier, O., Bilban, M., Bagot D'Arc, M., & Daculsi, G. (2009). Comparison of two bone substitute biomaterials consisting of a mixture of fibrin sealant (Tisseel®) and MBCP™ (TricOs ®) with an autograft in sinus lift surgery in sheep. *Clinical Oral Implants Research*, *20*, 1133–1139.

Sauerbier, S., Stricker, A., Kuschnierz, J., Bühler, F., Oshima, T., Xavier, S. P., Schmelzeisen, R., & Gutwald, R. (2010). In vivo comparison of hard tissue regeneration with human mesenchymal stem cells processed with either the ficoll method or the BMAC method. *Tissue Engineering - Part C: Methods*, *16*, 215–223.

Sauerbier, S., Stubbe, K., Maglione, M., Haberstroh, J., Kuschnierz, J., Oshima, T., Xavier, S. P., Brunnberg, L., Schmelzeisen, R., & Gutwald, R. (2010). Mesenchymal stem cells and bovine bone mineral in sinus lift procedures-an experimental study in sheep. *Tissue Engineering - Part C: Methods*, *16*, 1033–1039.

Scala, A., Botticelli, D., Faeda, R. S., Garcia Rangel, I., Américo de Oliveira, J., & Lang, N. P. (2012). Lack of influence of the Schneiderian membrane in forming new bone apical to implants simultaneously installed with sinus floor elevation: An experimental study in monkeys. *Clinical Oral Implants Research*, *23*, 175–181.

Schlegel, K. A., Fichtner, G., Schultze-Mosgau, S., & Wiltfang, J. (2003). Histologic findings in sinus augmentation with autogenous bone chips versus a bovine bone substitute. *The International Journal of Oral & Maxillofacial Implants*, 18, 53–58.

Schmitt, C. M., Doering, H., Schmidt, T., Lutz, R., Neukam, F. W., & Schlegel, K. A. (2013). Histological results after maxillary sinus augmentation with Straumann® BoneCeramic, bio-Oss®, puros®, and autologous bone. A randomized controlled clinical trial. *Clinical Oral Implants Research*, 24, 576–585.

Shanbhag, S., Shanbhag, V., & Stavropoulos, A. (2014). Volume changes of maxillary sinus augmentations over time: A systematic review. *The International Journal of Oral & Maxillofacial Implants*, 29, 881–892.

Sharan, A., & Madjar, D. (2008). Maxillary sinus pneumatization following extractions: A radiographic study. *The International Journal of Oral & Maxillofacial Implants*, 23, 48–56.

Silness, J., & Löe, H. (1964). Periodontal disease in pregnancy II. Correlation between oral hygiene and periodontal condition. *Acta Odontologica Scandinavica*, 22, 121–135.

Srouji, S., Ben-David, D., Lotan, R., Riminucci, M., Livne, E., & Bianco, P. (2010). The innate osteogenic potential of the maxillary sinus (Schneiderian) membrane: An ectopic tissue transplant model simulating sinus lifting. *International Journal of Oral and Maxillofacial Surgery*, 39, 793–801.

Starch-Jensen, T., Mordenfeld, A., Becktor, J. P., & Jensen, S. S. (2018). Maxillary sinus floor augmentation with synthetic bone substitutes compared with other grafting materials: A systematic review and meta-analysis. *Implant Dentistry*, 27, 363–374.

Stumbras, A., Krukis, M. M., Januzis, G., & Juodzbalys, G. (2019). Regenerative bone potential after sinus floor elevation using various bone graft materials: A systematic review. *Quintessence International*, 50, 548–558.

Tolstunov, L., Thai, D., & Arellano, L. (2012). Implant-guided volumetric analysis of edentulous maxillary bone with cone-beam computerized tomography scan. Maxillary sinus pneumatization classification. *Journal of Oral Implantology*, 38, 377–390.

Tomruk, C. O., Sençift, M. K., & Capar, G. D. (2016). Prevalence of sinus floor elevation procedures and survival rates of implants placed in the posterior maxilla. *Biotechnology and Biotechnological Equipment*, 30, 134–139.

Truedsson, A., Hjalte, K., Sunzel, B., & Warfvinge, G. (2013). Maxillary sinus augmentation with iliac autograft - A health-economic analysis. *Clinical Oral Implants Research*, 24, 1088–1093.

Van Dijk, L. A., Barrère-De Groot, F., Rosenberg, A. J. W. P., Pelletier, M., Christou, C., De Bruijn, J. D., & Walsh, W. R. (2020). MagnetOs, Vitoss, and Novabone in a multi-endpoint study of posterolateral fusion: A true fusion or not? *Clinical Spine Surgery*, 33, E276–E287.

van Dijk, L. A., Duan, R., Luo, X., Barbieri, D., Pelletier, M., Christou, C., Rosenberg, A. J. W. P., Yuan, H., Barrèrre-de Groot, F., Walsh, W. R., & de Bruijn, J. D. (2018). Biphasic calcium phosphate with submicron surface topography in an ovine model of instrumented posterolateral spinal fusion. *JOR Spine*, 1, e1039.

Yang, C., Zhao, C., Wang, X., Shi, M., Zhu, Y., Jing, L., Wu, C., & Chang, J. (2019). Stimulation of osteogenesis and angiogenesis by micro/nano hierarchical hydroxyapatite: Via macrophage immunomodulation. *Nanoscale*, 11, 17699–17708.

Yuan, H., Fernandes, H., Habibovic, P., De Boer, J., Barradas, A. M. C., De Ruiter, A., Walsh, W. R., Van Blitterswijk, C. A., & De Bruijn, J. D. (2010). Osteoinductive ceramics as a synthetic alternative to autologous bone grafting. *Proceedings of the National Academy of Sciences of the United States of America*, 107, 13614–13619.

SUPPORTING INFORMATION

Additional supporting information can be found online in the Supporting Information section at the end of this article.